American Mineralogist, Volume 84, pages 528–535, 1999

New kinetic model for the nanocrystalline anatase-to-rutile transformation revealing rate dependence on number of particles

HENGZHONG ZHANG* AND JILLIAN F. BANFIELD

Department of Geology and Geophysics, University of Wisconsin-Madison, 1215 West Dayton Street, Madison, Wisconsin 53706, U.S.A.

ABSTRACT

Existing kinetic models are unable to describe published experimental data for the anatase-to-rutile phase transformation in nanocrystalline samples. A new kinetic model is proposed that combines interface nucleation at certain contact areas between two anatase particles and formation and growth of rutile nuclei. Kinetic equations, incorporating mass-balance considerations, derived for this ''interface nucleation and constant growth'' model fit the experimental data of Gribb and Banfield (1997) fairly well. Results confirm that the transformation is second order with respect to the number of particles of anatase. Over shorter reaction times, the net transformation rate is determined by the rate of nucleation, which is initiated from rutile-like structural elements in the contact area. The activation energy of 165.6 ± 1.1 kJ/mol for rutile nucleation within nanocrystalline anatase particles is much lower than values previously measured for rutile nucleation in coarse anatase samples (>330 kJ/mol). Nuclei growth proceeds at a constant rate with a very small activation barrier. Over longer reaction times, the net transformation rate is determined both by nucleation and nuclei growth. Results quantitatively explain the origin of the size dependence of phase transformation rates in this system.

INTRODUCTION

Anatase and rutile are the most common of the seven or more TiO_2 polymorphs. Anatase, rutile, brookite, and TiO_2 (B) have been reported in nature to date (Banfield and Veblen 1992). All seven polymorphs are constructed from octahedrally coordinated Ti. Anatase is the most common product of low-temperature synthesis pathways, and is an important component of nanocrystalline materials developed for gas-phase separation and catalysis (Amores et al. 1995).

Both in nature, and in materials applications that involve heating, anatase coarsens and transforms to rutile (Banfield et al. 1993). The stability of anatase with respect to rutile is particle size dependent, with a stability reversal occurring at ~10–15 nm diameter (Gribb and Banfield 1997; Zhang and Banfield 1998a, 1998b). The phase transformation is reconstructive and requires repositioning of both Ti cations and a change in the oxygen arrangement.

Numerous researchers have investigated the kinetics of the anatase-to-rutile phase transformation (Table 1). While most past studies used rather coarsely crystalline anatase samples, recent studies mainly concentrated on nanocrystalline anatase. In these recent studies, factors affecting the transformation, such as temperature, pressure, particle size, additive/dopant, and hydrothermal condition were investigated (Banfield et al. 1993; Kumar et al. 1993a, 1993b; Ding et al. 1994; Amores et al. 1995; Liao et al. 1995; Ding et al. 1996; Bacsa and Gratzel 1996; Gribb and Banfield 1997). Comparison of these studies clearly demonstrates a strong size dependence for the transformation rate. In one case, a linear relationship between the coarsening and phase transformation rates was reported (Gribb and Banfield 1997).

Several kinetic models (Table 2) have been used to describe the experimental observations. Usually, one model best fits each specific study. However, Shannon and Pask (1965) showed that four different models were equally applicable. Each kinetic model is pertinent only to the specified transformation mechanism. The summary in Table 2 suggests that the style of nucleation, and growth for the transformation is highly temperature dependent and sample specific. For coarsely crystalline anatase, Shannon and Pask (1964) proposed a mechanism involving surface nucleation and described an intermediate level of topotaxy associated with the inheritance of a distorted oxygen framework. Penn and Banfield (1999) report that the atomic mechanism (atomic displacements) for the transformation in nanocrystals at 523 K is essentially identical to that occurring at 1173 K in millimeter-sized materials. The activation energy reported by Shannon and Pask was comparable to activation energies of most prior studies [exceeding ~400 kJ/mol; the exception being a value of 147 kJ/mol reported by Kumar et al. (1993a) for ultrafine anatase].

In this paper, we refine the kinetic analysis of the an-

* E-mail: hzhang@geology.wisc.edu

0003–004X/99/0004–0528$05.00

TABLE 1. Kinetic study of phase transformation of anatase to rutile

Year and author(s)	Sample: Preparation	Sample: Size (μm)	Sample: Additive/ impurity	Temperature (K)	Kinetic model*	E_a (kJ/mol)
1958 Czanderna	Ti + NH_3 + H_2O + H_2O_2	40 m^2/g (~0.04)		908–1001	2	377, 460
1961 Rao	same as above			898–971	1	335
1962 Suzuki	from $TiCl_4$	0.09–1	LiCl	1023–1073	1	460–485 (w/o add., in air) 377 (w/o add., in O_2) 628 (w/add.)
1965 Shannon	commercial	0.05–0.3	SO_3, P_2O_5	1323–1355	3–6	418–837
1969 Suzuki	sulfate and chloride process	0.2–0.7		1073–1153	7 (n = 0.34–1.61)	439, 448
1972 Heald	commercial		Fe_2O_3	1173–1273	3	519
1975 MacKenzie	sulfate process	~0.01	CuO, MnO_2, Fe_2O_3, LiF, Li_2CO_3	1118–1318	3	469 (w/o add.)† 636–724 (w/add.)†
1983 Hishita	commercial	0.05–0.14	rare earth oxides	1143–1258	7 (n = 0.93–1.87)	519 (w/o add.) 577 (w/add.)
1993 Kumar	sol-gel	~0.01		663–743	7 (n = 0.66)	147
1993 Banfield	sol-gel	nm	Cr, Y, Ta	738–973	1‡	268 197–209 (w/add.)
1997 Gribb	sol-gel	~6 nm		738–798		

* See Table 2.
† Original paper has mistakes in units.
‡ Only fit to data in early reaction time.

atase-to-rutile phase transformation, primarily using data of Gribb and Banfield (1997). The data were collected for synthetic nanocrystalline anatase prepared by a sol-gel method (Gribb and Banfield 1997). The as-prepared particle size of anatase samples was about 6 nm in diameter. Kinetic experiments were carried out at 738, 753, 773, and 798 K after a pretreatment at 598 K for 2 h (designed to remove most surface-bound water). Particle size and fraction of transformation in reacted samples (see Figs. 2–4 of Gribb and Banfield 1997) were determined by X-ray diffraction (XRD). Using these data for the present analysis, the kinetic law describing the phase transformation of nanocrystalline particles was established. A new kinetic model is proposed that combines interface nucleation and constant growth rate.

EXTENDED ANALYSIS OF DATA OF GRIBB AND BANFIELD (1997)

Shown on Figure 1 are plots of the left-hand sides (LHS) of various kinetic equations (models 1–6 of Table 2) vs. time using the experimental data of Gribb and Banfield (1997). Linearity of a plot is expected if the model fits the experimental data. Non-linearity of the plots indicate the invalidity of these models.

The Johnson-Mehl-Kolmogorov-Avrami (JMKA) equation is widely used to describe solid-state phase transformations (Borg and Dienes 1992; Lu 1996; Weinberg et al. 1997). Figure 2 shows the JMKA plot of the experimental data of Gribb and Banfield (1997). If the JMKA equation is applicable, a straight line should be generated in the plot, and the slope of the line can be used to infer the transformation mechanism (Borg and Dienes 1992). Varying and very low slopes of the plots in Figure 2 indicate the invalidity of the JMKA equation. The JMKA model assumes that nucleation is uniform in space but random in time, and furthermore that samples are of infinite size (Weinberg 1991). This third assumption makes application of this model to nanocrystalline anatase particles, which are of finite (and very small) sizes, physically unrealistic.

Weinberg et al. (1997) made several modifications to the JMKA theory, including consideration of surface nucleation and the effect of finite size (Weinberg 1991). According to Figure 7 of Weinberg (1991), the curve of the fraction of transformation vs. time is sigmoidal for a surface-nucleated sphere, and the corresponding JMKA plot has a slope between 1.5 and 4.5. The non-sigmoidal shape of the transformation data of Gribb and Banfield (1997) and the low slopes of the JMKA plots (Fig. 2) show that the modified JMKA equation is also invalid.

Distinction between the study of Gribb and Banfield (1997) and most others (Table 1) lies mainly in the particle size, the temperature range, and the experimental duration. Gribb and Banfield used anatase samples consisting of ultrafine particles, lower temperatures (738–798 K), and long duration experiments (up to ~800 h). The invalidity of previously employed kinetic models demonstrates that the style of nucleation and growth must be specific for the transformation of nanocrystalline anatase particles at lower temperatures.

MASS BALANCE DURING PHASE TRANSFORMATION

As discussed above, the phase transformation behavior of nanocrystalline anatase particles cannot be described by conventional kinetic models. A nanocrystalline particle is several tens to hundreds of times larger than a small molecule, but far smaller than a macroscopic crystallite. In a molecular reaction, the reaction rate is related to the

TABLE 2. Kinetic models describing phase transformation of anatase to rutile

Model	Equation*	Reference
1. Standard 1st order	$\ln(1-\alpha) = -kt$	Rao 1961; Suzuki and Kotera 1962; Banfield et al. 1993
2. Standard 2nd order	$\frac{1}{(1-\alpha)} - 1 = kt$	Czanderna et al. 1958
3. Contracting spherical interface	$(1-\alpha)^{1/3} - 1 = kt$	Shannon and Pask 1965; Heald et al. 1972; MacKenzie 1975
4. Nucleation and growth of overlapping nuclei	$[-\ln(1-\alpha)]^{1/3} = kt$	Shannon and Pask 1965
5. One dimensional, linear, branching nuclei and a constant growth	$\ln \alpha = kt + \text{const.}$	Shannon and Pask 1965
6. Random nucleation and rapid growth	$\ln(1-\alpha) = kt$	Shannon and Pask 1965
7. JMKA†	$\ln[-\ln(1-\alpha)] = n\ln t + \ln b$	Suzuki and Tukuda 1969; Hishita et al. 1983; Kumar et al. 1993

* α = fraction of transformation, t = time, and k = kinetic constant.
† b = a constant, and n = a parameter relevant to transformation mechanism (Borg and Dienes 1992).

concentration of the molecules. By analogy, we suggest that phase transformation rate of nanocrystalline anatase is related to the number of particles of anatase in a given volume (the ''concentration'' of anatase particles). The number of particles is derived below.

Nanocrystalline anatase particles that had transformed partially to rutile were only observed rarely in the experiments (Gribb and Banfield 1997). This implies that rutile growth was rapid after rutile nucleated. Suppose that the initial particle size and number of particles of anatase are, respectively, D_0 and N_0 at $t = 0$. After reacting for a period of time, t, the particle size and number of particles of anatase become, respectively, D_a and N_a, and those of rutile are, respectively, D_r and N_r. According to the principle of mass balance:

$$\frac{4}{3}\pi\left(\frac{D_0}{2}\right)^3 \cdot N_0 \cdot \rho_a = \frac{4}{3}\pi\left(\frac{D_a}{2}\right)^3 \cdot N_a \cdot \rho_a + \frac{4}{3}\pi\left(\frac{D_r}{2}\right)^3 \cdot N_r \cdot \rho_r \quad (1)$$

where ρ_a and ρ_r represent the densities of anatase and rutile, respectively. The fraction of transformation, α, is the following:

$$\alpha = \frac{\frac{4}{3}\pi\left(\frac{D_0}{2}\right)^3 \cdot N_0 \cdot \rho_a - \frac{4}{3}\pi\left(\frac{D_a}{2}\right)^3 \cdot N_a \cdot \rho_a}{\frac{4}{3}\pi\left(\frac{D_0}{2}\right)^3 \cdot N_0 \cdot \rho_a} = 1 - \frac{N_a}{N_0}\left(\frac{D_a}{D_0}\right)^3. \quad (2)$$

From Equations 1 and 2, we obtain:

$$\frac{N_a}{N_0} = (1-\alpha) \cdot \left(\frac{D_0}{D_a}\right)^3 \quad (3)$$

$$\frac{N_r}{N_0} = \alpha \cdot \frac{\rho_a}{\rho_r} \cdot \left(\frac{D_0}{D_r}\right)^3. \quad (4)$$

Figure 3 shows the number of particles of anatase calculated from Equation 3. A significant decrease in the number of anatase particles occurs after reacting for a few hours to tens of hours.

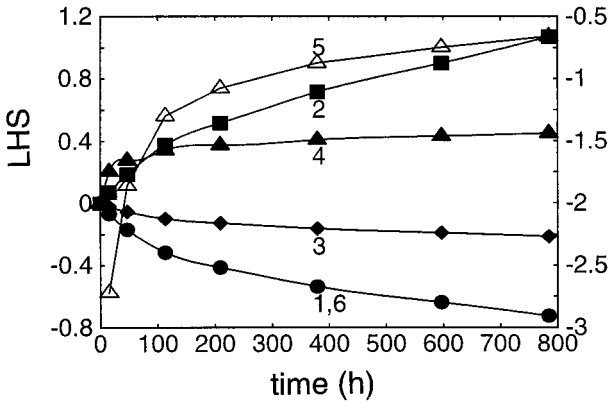

FIGURE 1. Plots of the left-hand side (LHS) of Equations 1–6 (Table 2) vs. time at 738 K. Numbers on the graph indicate the model number (Table 2) (model 5 uses the right axis of the diagram). Lines are guides for the eyes. Data of Gribb and Banfield (1997).

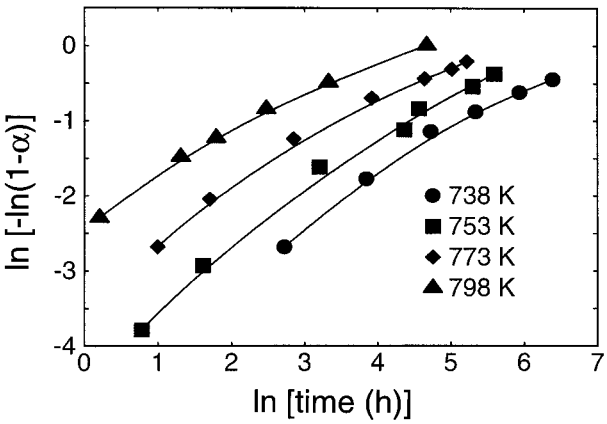

FIGURE 2. JMKA plots of the transformation data at various temperatures; non-linearity is observed. The slopes of the curves range from 0.37 to 0.88. Data of Gribb and Banfield (1997).

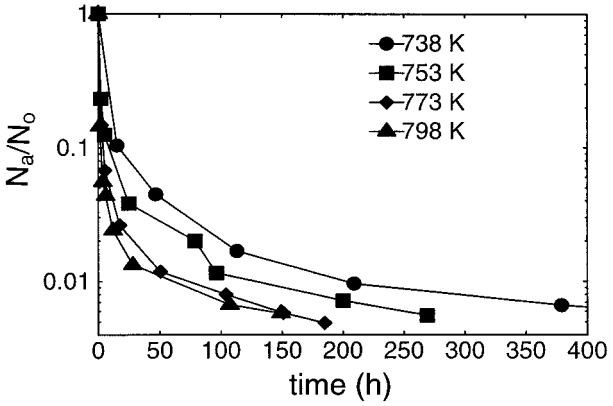

FIGURE 3. Plot of the numbers of particles of anatase (normalized to the initial number of particles of anatase) vs. time at various temperatures. Lines are guides for the eyes.

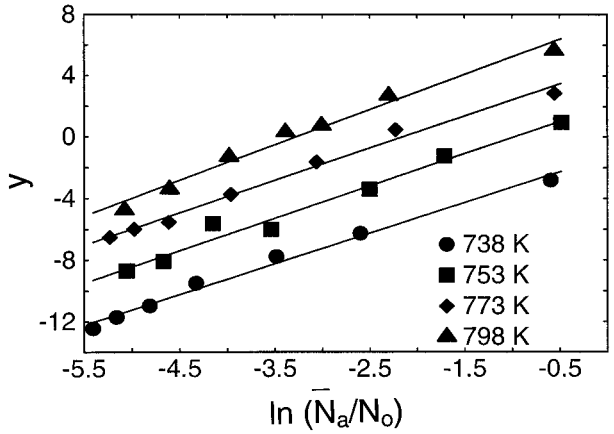

FIGURE 4. Plot of $y = \ln[-\Delta(N_a/N_0)/\Delta t]$ vs. $\ln(\overline{N}_a/N_0)$. For clarity, the y values at 753, 773, and 798 K were shifted up 2, 4, and 6 units, respectively.

REACTION ORDER BY DIFFERENTIAL METHOD

It is assumed that the rate of the phase transformation of nanocrystalline anatase particles is n^{th} order with respect to the number of particles of anatase. Accordingly, the transformation rate, the number of particles of anatase transformed in a unit time, can be written as:

$$-\frac{dN_a}{dt} = kN_a^n \tag{5}$$

where k is a kinetic constant relevant to temperature and volume of the sample. Replacing N_a with N_a/N_0, we get:

$$-\frac{d(N_a/N_0)}{dt} = k_1(N_a/N_0)^n \tag{6}$$

where $k_1 = kN_0^{n-1}$. A logarithm transformation of Equation 6 gives:

$$\ln\left[-\frac{d(N_a/N_0)}{dt}\right] = \ln k_1 + n \ln(N_a/N_0). \tag{7}$$

The quantity $d(N_a/N_0)/dt$ can be approximated by $\Delta(N_a/N_0)/\Delta t$, calculated from two adjacent data points in Figure 3 at the mean of the numbers of particles of anatase ($\overline{N}_a/N_0$). Figure 4 shows the plot of the data thus obtained. It can be seen that the plots are of very good linearity. The slopes of the four linear regression lines are 1.99, 2.10, 2.10, and 2.30 for 738, 753, 773, and 798 K, respectively, suggesting that $n = 2$. Since a solid-state phase transformation typically proceeds via nucleation and growth, Equation 5 with $n = 2$ can be interpreted as indicating that the net transformation rate is limited by nucleation of rutile in the contact area (interface) of two anatase particles, whereas the nucleation rate is determined by the probability of contact of two anatase particles.

We now further examine the integration of Equation 6 with $n = 2$:

$$\frac{1}{(N_a/N_0)} - 1 = k_1 t. \tag{8}$$

Combining Equation 8 with Equation 3, we obtain:

$$\frac{1}{(1-\alpha)(D_0/D_a)^3} - 1 = k_1 t. \tag{9}$$

Figure 5 shows the plot of the left-hand side of Equation 9 vs. time at various temperatures. It is seen that linearity is observed over shorter reaction times. Over longer reaction times, however, the plot deviates from linearity, indicating that other factors such as nuclei growth may become important in addition to the interface nucleation.

KINETIC MODEL FOR PHASE TRANSFORMATION

It has been shown that, over shorter reaction times, interface nucleation controls the net transformation rate, so the rate is second order with respect to the number of particles of anatase. Over longer reaction times, experimental results deviate from the law (Fig. 5). We attribute this to the requirement for a finite growth period of the

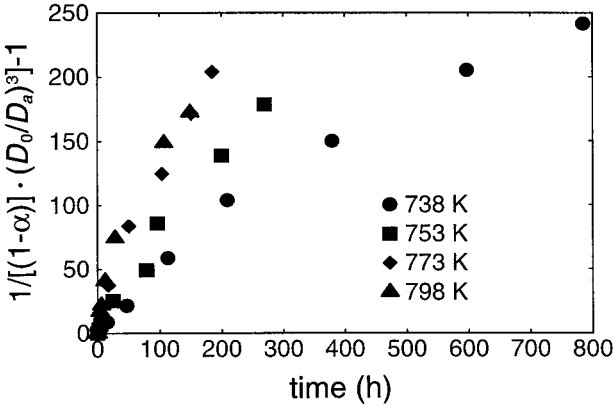

FIGURE 5. Plot of $1/[(1-\alpha)(D_0/D_a)^3]-1$ vs. time at various temperatures.

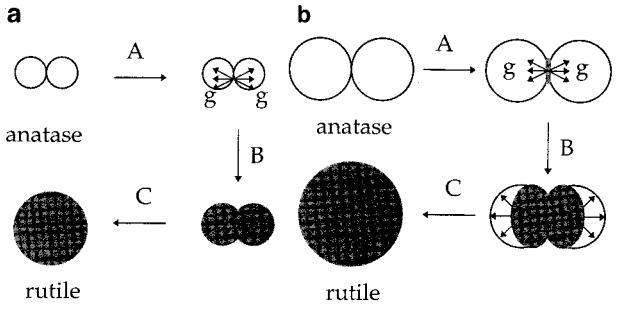

FIGURE 6. Diagram showing steps involved in the phase transformation of nanocrystalline anatase particles over shorter reaction times (**a**) and over longer reaction times (**b**). The g is the nuclei growth rate.

rutile nuclei as anatase particles enlarge. Consequently, a kinetic model incorporating both interface nucleation and nuclei growth is proposed below (Fig. 6).

Step A, interface nucleation

Nucleation of rutile starts within the interface between two contacting anatase particles, and the nucleation rate is determined by the probability of contact of two anatase particles, i.e., by the square of the ''concentration'' of anatase particles (the number of particles of anatase in a given volume). The nucleation rate, the number of particles of anatase nucleated (N_a^*) in unit time, then can be represented by:

$$-\frac{dN_a^*}{dt} = kN_a^2 \tag{10}$$

where k is a kinetic constant associated with the interface nucleation.

Step B, nuclei growth

As for any nucleation event, the formation of a stable nucleus is dependent upon interfacial energy. The critical size for rutile is on the order of 10 nm (Gribb and Banfield 1997). Fluctuation of a rutile nucleus within an anatase particle of around this size would almost certainly result in rapid transformation of the entire particle (Fig. 6a), removing the interfacial energy contribution. However, more protracted rutile nuclei growth will be required to achieve this result as the anatase particle grows (Fig. 6b).

Step C, formation of a rutile particle

This step happens simultaneously with step B, and involves growth at the particle-particle neck from constituents evidently provided by surface diffusion.

In the following, kinetic equations are derived according to the transformation sequence proposed above.

Over shorter reaction times (Fig. 6a), nuclei growth can be considered instantaneous and the net phase transformation rate ($-dN_a/dt$) is limited by the interface nucleation (Step A). Thus, $-dN_a/dt = -dN_a^*/dt$ (Eq. 10; the integrated form is the same as Eq. 9).

Over longer reaction times (Fig. 6b), a number of ($-dN_a^*/dt$) anatase particles are nucleated in unit time (step A). However, an additional time, τ, is needed for the nuclei to grow to the entire volume (step B) with simultaneous growth of the rutile particle (step C). Obviously, the larger the particle, the longer the additional time. Thus τ can be represented by $\tau = k'(D_a/D_0)$, where k' is a constant. The net transformation rate, the number of particles of anatase transformed (N_a) in unit time, then can be expressed as:

$$-\frac{dN_a}{dt} = -\frac{dN_a^*/dt}{1+\tau} = \frac{kN_a^2}{1+\tau} \tag{11}$$

or

$$-\frac{d(N_a/N_0)}{dt} = \frac{k_1(N_a/N_0)^2}{1+\tau} = \frac{k_1(N_a/N_0)^2}{1+k'(D_a/D_0)}. \tag{12}$$

We assume that over sufficiently long reaction times $\tau \gg 1$, so Equation 12 can be approximated by:

$$-\frac{d(N_a/N_0)}{dt} = \frac{k_1}{k'}\cdot\frac{(N_a/N_0)^2}{(D_a/D_0)}. \tag{13}$$

Integration of Equation 13 relies on the time dependence of the particle size of anatase, or the particle coarsening behavior. For polycrystalline materials, grain growth is commonly described by the equation (Lu 1996):

$$D - D_0 = k''t^{1/m} \tag{14}$$

where k'' is a constant, m an exponent representing the grain growth behavior that generally falls between 2 and 4. Equation 14 also has been used to describe the coarsening behavior of nanocrystalline particles (Lu 1996). A non-linear least-squares fit of the particle size data of anatase (Fig. 3 of Gribb and Banfield 1997) with Equation 14 gives m = 3.5, 3.1, 3.7, and 5.1 for 738, 753, 773, and 798 K, respectively. The Marquardt-Levenberg Algorithm was employed in the fitting, and each data point was weighted equally because experimental errors are not known for all the data. The m value for 798 K is considered erroneous due to inclusion of the last two data points, which appear to be in error. Specifically, the original 798 K data set shows discontinuities in trends for both rutile and anatase not found in any other experiments. In part, this may be due to difficulty in measurement of the size of larger crystals via peak broadening analysis. If the last two data points from 798 K are omitted, the value for m is 3.3. Thus, a value of m between 3 and 4 is reasonable for nanocrystalline anatase particles. The lines on Figure 7 are the least-square fits of the coarsening data of anatase at fixed m = 3 (the last two data points from 798 K are included in Fig. 7, but they were not adopted in the fitting). The values of k'' obtained from the fit are listed in Table 3.

Rearrangement of Equation 14 yields:

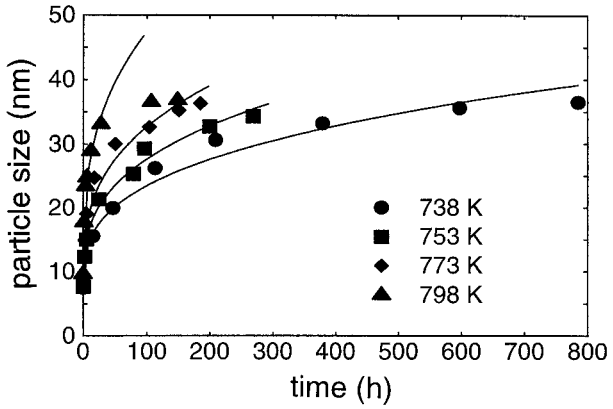

FIGURE 7. Least-squares fit of particle size of anatase based on Equation 14 ($m = 3$).

$$\frac{D}{D_0} = 1 + \frac{k''}{D_0}t^{1/m}. \quad (15)$$

Over a sufficiently long period of time, the second term in the right-hand side of Equation 15 is far greater than 1. Thus Equation 13 can be approximated by:

$$-\frac{d(N_a/N_0)}{dt} = k''' \cdot \frac{(N_a/N_0)^2}{t^{1/m}} \quad (16)$$

where $k''' = (k_1 D_0)/(k'k'')$ is an apparent kinetic constant relevant to the interface nucleation ($k_1 = kN_0$, Eq. 10), nuclei growth (k', Eq. 12), initial anatase particle size (D_0), and the particle coarsening (k'', Eq. 14). Integrating Equation 16, and inserting Equation 3 into the equation thus obtained, we arrive at:

$$\frac{1}{(1-\alpha)(D_0/D_a)^3} - 1 = k_2 t^{(m-1)/m} \quad (17)$$

where

$$k_2 = \frac{m}{m-1} \cdot k''' = \frac{m}{m-1} \cdot \frac{k_1 D_0}{k'k''} \quad (18)$$

Derivation of model parameters

In terms of Equation 9, over shorter reaction times:

$$\ln\left[\frac{1}{(1-\alpha)(D_0/D_a)^3} - 1\right] = \ln k_1 + \ln t. \quad (19)$$

In terms of Equation 17, over longer reaction times:

$$\ln\left[\frac{1}{(1-\alpha)(D_0/D_a)^3} - 1\right] = \ln k_2 + \frac{m-1}{m}\ln t \quad (20)$$

where $m = 3$–4. The kinetic constants k_1 and k_2 can be obtained from a plot of the left-hand side of Equation 19 and/or 20 vs. ln(time) for the experimental data of Gribb and Banfield (1997) (Fig. 8). Table 3 shows that slope 1 (for shorter reaction times) and slope 2 (for longer reaction times) are reasonably close to the model values.

TABLE 3. Kinetic model parameters

Temperature (K)	738	753	773	798
Constant, k'' (nm/h$^{0.33}$)*	3.44	4.30	5.29	8.13
Slope 1†	0.96	0.84	0.90	0.84
Constant, k_1 (1/h)	0.59	1.73	2.64	5.13
Slope 2‡	0.65	0.70	0.68	0.56
Constant, k_2 (1/h$^{(m-1)/m}$)	3.29	3.43	5.65	10.58

* Of Equation 14 at $m = 3$.
† Slopes of lines in Figure 8 over shorter reaction times, model value 1 (Eq. 19).
‡ Slopes of lines in Figure 8 over longer reaction times, model value between 0.67 and 0.75 (Eq. 20 at $m = 3 - 4$).

DISCUSSION

Kinetic analysis indicates that over the temperature range 738–798 K, the phase transformation of nanocrystalline anatase particles proceeds in a sequence of interface nucleation followed by nuclei growth. Kinetic constants were obtained for this transformation (Table 3), and their temperature variation can be described by the Arrhenius equation:

$$\ln k = -\frac{E_a}{RT} + \ln k_0 \quad (21)$$

where E_a is activation energy, k_0 a material properties constant, R the universal gas constant (8.314 J/mol·K), and T the absolute temperature. From the Arrhenius plot of various kinetic constants (Fig. 9), we obtain: (1) the activation energy of interface nucleation, $E_a(k_1) = 165.6 \pm 1.1(1.7)$ kJ/mol; (2) the apparent activation energy, $E_a(k_2) = 100.0 \pm 0.9$ (0.9) kJ/mol; and (3) the activation energy of coarsening of anatase particles, $E_a(k'') = 68.6 \pm 0.3$ (0.4) kJ/mol. In each case, the standard deviation (or the largest deviation in the parentheses) was estimated from the deviation between the lnk and the fitting in Figure 9 using Equation 21.

According to Equations 18 and 21, we have:

$$E_a(k_2) = E_a(k_1) - E_a(k') - E_a(k'') \quad (22)$$

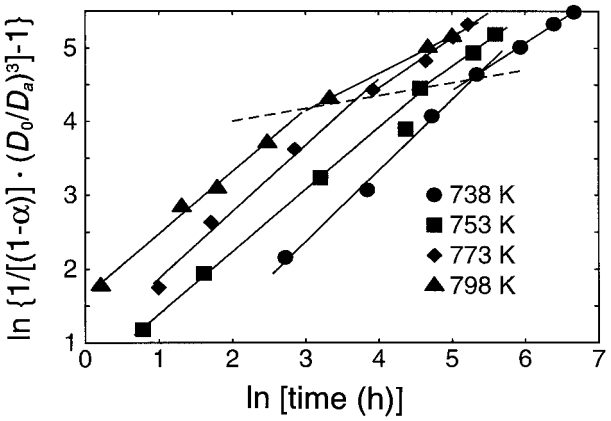

FIGURE 8. Plot of $\ln\{1/[(1-\alpha)(D_0/D_a)^3]-1\}$ vs. ln(time) at various temperatures. The dashed line approximately separates the shorter reaction time interval from the longer reaction time.

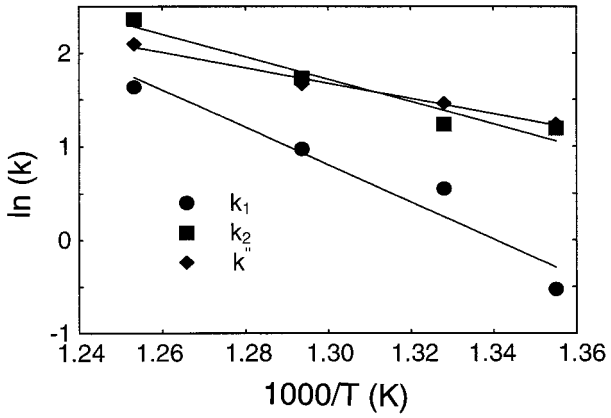

FIGURE 9. Arrhenius plot of various kinetic constants.

where $E_a(k')$ is the activation energy for the growth of nuclei. Insertion of $E_a(k_1)$, $E_a(k_2)$, and $E_a(kd'')$ into the above equation results in $E_a(k') = -3.0 \pm 2.3$ (3.0) kJ/mol, where the standard (or largest) deviation was accumulated from those of $E_a(k_1)$, $E_a(k_2)$, and $E_a(k'')$. Normally an activation energy is non-negative. Considering the errors generated in the data processing (as shown by the standard or largest deviation), as well as those inherent to the experiments, the low and slightly negative value of $E_a(k')$ can be interpreted as indicating that the activation energy for the nuclei growth is nearly zero. This means that the rate of the nuclei growth is a constant that is independent of temperature, i.e., the nuclei growth is not thermally activated. In Figure 8, the dashed line marks the approximate beginning of the longer reaction period at which Equation 13 becomes valid ($\tau \gg 1$). At this stage, the additional time, τ, must be the same for all temperatures. Read from Figure 7, the particle size of anatase on the dashed line is 31 ± 0, 29 ± 0, 30 ± 1, and 33 ± 1 nm at 738, 753, 773, and 798 K, respectively (errors are interpolation errors). These sizes are about the same. Consequently, the nuclei growth rate (g = size/τ) is about the same for all temperatures, confirming the result from the activation energy analysis. Therefore, the model proposed in this study can be termed ''interface nucleation and constant growth.''

Extensive sample characterization by Gribb and Banfield (1997) indicated that partially reacted anatase particles are found only rarely. This can be readily explained over shorter reaction times in which rutile nuclei on the interface grow rapidly to consume the two contact anatase particles because of their small particle size (Fig. 6a). Thus nanocrystalline particles detected are either anatase or rutile. Over longer reaction times (Fig. 6b), although the growth of nuclei takes additional time, partially reacted anatase particles are rare because the number of anatase particles has decreased dramatically (Fig. 3).

In the standard JMKA theory, nucleation is usually considered in terms of probabilities and is treated as uniform in space and random in time. Obviously, such a treatment is not reasonable for interface nucleation because interface nucleation requires contact between two anatase particles, and the nucleation rate (Eq. 10) is time dependent. Amores et al. (1995) proposed a ''sintering-induced phase transformation'' mechanism that is somewhat similar to the process proposed here. Nucleation on the interface of two anatase particles was explained by these authors as initiated by the large heat evolved during the sintering of two anatase particles.

Penn and Banfield (1998) used high-resolution transmission electron microscopy to show that twins formed in anatase coarsened under hydrothermal conditions. Analysis of the atomic details of the {112} anatase twin composition plane revealed that it contained structural elements (two octahedra-wide chains) that are common to rutile. Based on this observation, evidence for rutile nuclei at twin composition planes, and topotactic details, Penn and Banfield (1999) proposed a detailed atomic phase transformation mechanism. The essential features of this mechanism are initial rutile formation by atomic displacements involving half the sites comprising the twin composition plane, followed by a chain reaction due to destabilization of the surrounding anatase. Despite the fairly drastic structural change required for conversion of anatase to rutile, only 7 out of 24 Ti-O bonds are ruptured (for bulk material). Inherent in this model are implications of a lowered activation barrier for rutile nucleation due to the interface structure, and subsequent rapid rutile growth (implying a low activation barrier for rutile growth once nucleation is accomplished).

The connection between phase transformation rate and twinning requires a mechanism for the production of twins. In the work of Penn and Banfield (1999), twin formation occurred as a consequence of crystal growth via oriented attachment. This mechanism involves either rotation of touching particles to eliminate surface tension associated with the interface, or attachment of particles brought into appropriate contact during coarsening. This growth mechanism may also operate during coarsening of dry powders, but our preliminary observations suggest it is not common. However, it is probable that the lowering of the activation barrier for rutile nucleation does not require extensive planar arrays of clusters structurally related to rutile; smaller clusters may suffice. The critical requirement may simply be that adjacent anatase particles are oriented such that their octahedra tilt in opposing directions. Thus, interfaces between fortuitously oriented particles in dry aggregates may serve essentially the same role in promoting rutile nucleation. It is also possible that heat of recrystallization contributes to this process. However, some experiments of Gribb and Banfield (1997) were of very long duration (Fig. 7), so heat evolved during particle coarsening should be dispersed quite readily. Thus, the role of structural elements introduced at particle-particle contacts is considered to be quite significant in explaining the observed dependence of the rate on the number of particles of anatase (and thus, their size).

The kinetic model (Fig. 6) also explains the commonly observed dependence of transformation rates on details

of the materials synthesis pathway (Gribb and Banfield 1997, and unpublished data). Aggregates characterized by different nanocrystal packing arrangements will vary in their number of particle-particle contacts, and thus in abundance of favorable rutile nucleation sites.

In short, the kinetic model proposed in this study quantitatively represents the basic nature of the transformation process of nanocrystalline anatase particles: interface nucleation and constant nuclei growth. Rutile nucleation originates from some rutile-like structural elements created by contact between anatase particles in different orientations. This model describes the experimental data of Gribb and Banfield (1997) fairly well.

ACKNOWLEDGMENTS

Thanks are extended to R. Lee Penn for helpful discussion and two anonymous reviewers. Financial support for this study was provided by National Science Foundation grant number EAR-9508171.

REFERENCES CITED

Amores, J.M.G., Escribano, V.S., and Busca, G. (1995) Anatase crystal growth and phase transformation to rutile in high-area TiO_2, MoO_3-TiO_2 and other TiO_2-supported oxide catalytic systems. Journal of Materials Chemistry, 5, 1245–1249.

Bacsa, R.R. and Gratzel, M. (1996) Rutile formation in hydrothermally crystallized nanosized titania. Journal of the American Ceramic Society, 79, 2185–2188.

Banfield, J.F. and Veblen, D.R. (1992) Conversion of perovskite to anatase and TiO_2(B): A TEM study and the use of fundamental building blocks for understanding relationship among the TiO_2 minerals. American Mineralogist, 77, 545–557.

Banfield, J.F., Bischoff, B.L., and Anderson, M.A. (1993) TiO_2 accessory minerals: coarsening, and transformation kinetics in pure and doped synthetic nanocrystalline materials. Chemical Geology, 110, 211–231.

Borg, R.J. and Dienes, G.J. (1992) The Physical Chemistry of Solids, 584 p. Academic Press, Boston.

Czanderna, A.W., Rao, C.N.R., and Honig, J.M. (1958) The anatase-rutile transition Part: I. Kinetics of the transformation of pure anatase. Transactions of the Faraday Society. 54, 1069–1073.

Ding, X.Z., Liu, L., Ma, X.M., Qi, Z.Z., and He, Y.Z. (1994) The influence of alumina dopant on the structural transformation of gel-derived nanometer titania powders. Journal of Materials Science Letters, 13, 462–464.

Ding, X.Z., Liu, X.H., and He, Y.Z. (1996) Grain size dependence of anatase-to-rutile structural transformation in gel-derived nanocrystalline titania powders. Journal of Materials Science Letters, 15, 1789–1791.

Gribb, A.A. and Banfield, J.F. (1997) Particle size effects on transformation kinetics and phase stability in nanocrystalline TiO_2. American Mineralogist, 82, 717–728.

Heald, E.F. and Weiss, C.W. (1972) Kinetics and mechanism of the anatase/rutile transformation, as catalyzed by ferric oxide and reducing conditions. American Mineralogist, 57, 10–23.

Hishita, S., Mutoh, I., Koumoto, K., and Yanagida, H. (1983) Inhibition mechanism of the anatase-rutile phase transformation by rare earth oxides. Ceramics International, 9, 41–47.

Kumar, K.N.P., Keizer, K., and Burggraaf, A.J. (1993a) Textural evolution and phase transformation in titania membranes: Part 1. Unsupported membranes. Journal of Materials Chemistry, 3, 1141–1149.

Kumar, K.N.P., Keizer, K., Burggraaf, A.J., Okubo, T., and Nagamoto, H. (1993b) Textural evolution and phase transformation in titania membranes: Part 2. Supported membranes. Journal of Materials Chemistry, 3, 1151–1159.

Liao, S.C., Pae, K.D., and Mayo, W.E. (1995) The effect of high pressure on phase transformation of nanocrystalline TiO_2 during hot-pressing. Nanostructured Materials, 5, 319–325.

Lu, K. (1996) Nanocrystalline metals crystallized from amorphous solids: nanocrystallization, structure, and properties. Materials Science and Engineering, R16, 161–221.

MacKenzie, K.J.D. (1975) The calcination of titania V. Kinetics and mechanism of the anatase-rutile transformation in the presence of additives. Transactions and Journal of the British Ceramic Society, 74, 77–84.

Penn, R.L. and Banfield, J.F. (1998) Oriented attachment and growth, twinning, polytypism, and formation of metastable phases: insights from nanocrystalline TiO_2. American Mineralogist, 83, 1077–1082.

———(1999) Formation of rutile nuclei at anatase {112} twin interfaces and the phase transformation mechanism in nanocrystalline titania. American Mineralogist, 84, in press.

Rao, C.N.R. (1961) Kinetics and thermodynamics of the crystal structure transformation of spetroscopically pure anatase to rutile. Canadian Journal of Chemistry, 39, 498–500.

Shannon, R.D. and Pask, J.A. (1964) Topotaxy in the anatase-rutile transformation. American Mineralogist, 49, 1707–1717.

———(1965) Kinetics of the anatase-rutile transformation. Journal of the American Ceramic Society, 48, 391–398.

Suzuki, A. and Kotera, Y. (1962) The kinetics of the transition of titanium dioxide. Bulletin of the Chemical Society of Japan, 35, 1353–1357.

Suzuki, A. and Tukuda, R. (1969) Kinetics of the transition of titanium dioxide prepared by sulfate process and chloride process. Bulletin of the Chemical Society of Japan, 42, 1853–1857.

Weinberg, M.C. (1991) Surface nucleated transformation kinetics in 2- and 3-dimensional finite systems. Journal of Non-Crystalline Solids, 134, 116–122.

Weinberg, M.C., Birnie, D.P. III, and Shneidman, V.A. (1997) Crystallization kinetics and the JMAK equation. Journal of Non-crystalline Solids, 219, 89–99.

Zhang, H. and Banfield, J.F. (1998a) Phase stability in the nanocrystalline TiO_2 system. In E. Ma, P. Bellon, M. Atzmon, and R. Trivedi, Eds., Phase Transformations and Systems Driven Far From Equilibrium, p. 619–624. Materials Research Society, Warrendale, Pennsylvania.

———(1998b) Thermodynamic analysis of phase stability of nanocrystalline titania. Journal of Materials Chemistry, 8, 2073–2076.

MANUSCRIPT RECEIVED JUNE 12, 1998
MANUSCRIPT ACCEPTED OCTOBER 17, 1998
PAPER HANDLED BY SIMON A.T. REDFERN